Published in "Journal of Polymer Science Part A:
Polymer Chemistry 48(3): 614-626, 2010"
which should be cited to refer to this work.

Poly(3-hexylthiophene)-*b*-poly(3-cyclohexylthiophene): Synthesis, Microphase Separation, Thin Film Transistors, and Photovoltaic Applications

PEI-TZU WU,[1,2] GUOQIANG REN,[1,2] FELIX S. KIM,[1,2] CHAOXU LI,[3] RAFFAELE MEZZENGA,[3,4] SAMSON A. JENEKHE[1,2]

[1]Department of Chemical Engineering, University of Washington, Seattle, Washington 98195-1750

[2]Department of Chemistry, University of Washington, Seattle, Washington 98195-1750

[3]Department of Physics and Fribourg Center for Nanomaterials, Fribourg University, Fribourg, Switzerland

[4]Nestlé Research Center, Vers-Chez-Les-Blanc, 1000 Lausanne 26, Switzerland

ABSTRACT: We report the synthesis, characterization, microphase separation, field-effect charge transport, and photovoltaic properties of regioregular poly(3-hexylthiophene)-*b*-poly(3-cyclohexylthiophene) (P3HT-*b*-P3cHT). Two compositions of P3HT-*b*-P3cHT (HcH63 and HcH77) were synthesized with weight-average molecular weights of 155,500 and 210,800 and polydispersity indices of 1.45 and 1.57, respectively. Solvent-casted HcH77 was found to self-assemble into nanowires with a width of 12.5 ± 0.9 nm and aspect ratios of 50–120, as observed by TEM imaging. HcH77 and HcH63 annealed 280 °C were observed by small angle X-ray scattering (SAXS) and wide angle X-ray scattering (WAXS) to be microphase-separated with characteristic length scales of 17.0–21.7 nm. The microphase-separated domains were shown to be crystalline with interlayer backbone (100) *d*-spacings of 1.69 and 1.40 nm, which correspond to the P3HT and P3cHT blocks, respectively. Field-effect transistors fabricated from P3HT-*b*-P3cHT thin films showed a mobility of holes (0.0019 cm^2/Vs) which is independent of thermal annealing. Bulk heterojunction solar cells based on HcH77/fullerene ($PC_{71}BM$) blend thin films had a maximum power conversion efficiency of 2.45% under 100 mW/cm^2 AM1.5 solar illumination in air. These results demonstrate that all-conjugated block copolymers are suitable semiconductors for applications in field-effect transistors and bulk heterojunction solar cells. © 2009 Wiley Periodicals, Inc. J Polym Sci Part A: Polym Chem 48: 614–626, 2010

KEYWORDS: conjugated polymers; diblock copolymers; microphase separation; polymer solar cells; SAXS; thin-film transistors; WAXS

INTRODUCTION Multicomponent-conjugated polymer systems,[1–26] especially polymer blends[1–7] and block copolymers,[8–20] offer the opportunity to tailor their electronic and optical properties to levels well beyond those possible in homopolymers and random/alternating copolymers. Most polythiophene-based multicomponent conjugated polymer systems investigated so far have been based on poly(3-hexylthiophene) (P3HT),[1,27,28] which is known to be a high mobility p-type polymer semiconductor[29,30] and a good donor component in fullerene-based bulk heterojunction (BHJ) solar cells.[31,32] Although binary blends of poly(3-alkylthiophene)s, exemplified by blends of P3HT with poly(3-decylthiophene) (P3DT)[1] or poly(3-octylthiophene) (P3OT),[4] have interesting electronic properties and charge carrier mobility that vary with blend composition,[1] random copolymers can have superior properties and more robust morphology.[4] Random copolythiophenes with a variety of substituted side chains such as hexyl, octyl, cyclohexyl, or 4-octylphenyl have been reported.[4,33–37] Because of their well-defined sequences, ordered chain architecture, and capability for self-assembly, block copolymers are especially attractive among multicomponent conjugated polymer systems. Block copolythiophenes with crystalline-amorphous diblock architecture incorporating poly(3-hexylthiophene) (P3HT) block have been reported.[38–40] The presence of amorphous domains in polymer semiconductors is not desirable for many electronic applications such as thin film transistors and photovoltaic cells.[41] To ensure crystallinity in microphase-separated domains, crystalline–crystalline diblock copolymers can be an appealing approach.[41] However, block copolythiophene systems have not yet been extensively studied and evaluated for electronic applications such as thin film transistors and photovoltaic cells.[33–40]

We report herein the synthesis, microphase separation, field-effect charge transport, and photovoltaic properties of regioregular poly(3-hexylthiophene)-*b*-poly(3-cyclohexylthiophene) (P3HT-*b*-P3cHT). Two compositions of P3HT-*b*-P3cHT,

denoted HcH63 and HcH77, were found to undergo microphase separation into two distinct crystalline domains as observed by temperature-dependent small-angle and wide-angle X-ray scattering (SAXS, WAXS). Bottom-contact field-effect transistors were fabricated and used to evaluate the carrier mobility of holes in P3HT-*b*-P3cHT thin films. Bulk heterojunction solar cells based on P3HT-*b*-P3cHT/fullerene blends were fabricated and used to study the photovoltaic properties of P3HT-*b*-P3cHT.

EXPERIMENTAL

Materials

3-Hexylthiophene, 2,5-dibromo-3-cyclohexylthiophene, anhydrous THF, isopropylmagnesium chloride (*i*-PrMgCl, 2M in THF), butylmagnesium chloride (BuMgCl, 2M in THF), [1,2-bis(diphenylphosphino)ethane]dichloronickel(II) [Ni(dppe)Cl_2], *N*-bromosuccinimide (NBS), and poly(3-hexylthiophene) were purchased from Sigma-Aldrich and were used as received. 2,5-Dibromo-3-hexylthiophene was synthesized following the literature method.[41,42] [6,6]–phenyl-C_{71} butyric acid methyl ester ($PC_{71}BM$, >99.0%) was purchased from American Dye Source (Quebec, Canada) and used as received. 1,2-dicholorobenzene (ODCB, anhydrous, > 99%, Aldrich) was degassed with nitrogen before use. Poly(3,4-thylenedioxythiophene):poly(styrene sulfonate) (PEDOT; Baytron P VP AI 4083) was purchased from H. C. Stark (Newton, MA) and passed through a 0.45-μm filter before spin-coating.

Polymer Synthesis

Poly(3-hexylthiophene)-block-*poly(3-cyclohexylthiophene) (HcH63 & HcH77)*

The molar feed ratio of 2,5-dibromo-3-hexylthiophene (HT) and 2,5-dibromo-3-cyclohexylthiophene (cHT) was 1:1 and 2:1 for the HcH63 and HcH77 samples, respectively. The molecular weight was controlled by fixing the ratio of the amount of Ni catalyst to the total monomer amount at 1:100. The typical synthesis procedure of HcH63 diblock copolymer (feed molar ratio of 1:1) was as follows: two round-bottomed flasks (250 mL) equipped with a three-neck stopcock were dried by heating under reduced pressure and cooled to room temperature. 2,5-Dibromo-3-hexylthiophene (1.038 g, 3.2 mmol) was placed in one flask under Ar, and then evacuated under reduced pressure to remove any moisture and oxygen inside. After anhydrous THF (45 mL) was added into the flask via a syringe, the solution was stirred at 0 °C. 2 M solution of *i*-PrMgCl in THF (1.6 mL, 3.2 mmol) was added via a syringe, and the mixture was stirred at 0 °C for 30 min (Solution 1). In the other flask, 2,5-dibromo-3-cyclohexylthiophene (1.032 g, 3.2 mmol) was first reacted with *i*-PrMgCl (1.6 mL, 3.2 mmol) (Solution 2) at 0 °C for 30 min, and then heated to 50 °C. Solution 1 was heated up to 50 °C and Ni(dppe)Cl_2 catalyst (33.8 mg, 0.064 mmol) was added in one portion. After stirring for 1 h, Solution 2 was transferred to Solution 1 via a double-tipped needle, and the resulting solution was stirred at 50 °C for overnight. The reaction was quenched by adding HCl solution (20 wt %) into the solution. The crude polymer was successively washed by Soxhlet extraction using methanol, acetone, and hexane. The solvent was removed by evaporation to give a purple solid (0.59 g, Yield: 55%). HcH77 with a molar feed ratio of 2:1 (HT:cHT) was also synthesized following the same procedure to give a purple solid (0.8 g, Yield: 65%) as the final product. The assignment of each proton resonance in the ^{1}H NMR spectra of HcH samples is as shown in Figure S1. Based on the integration of the peaks of the two resonance peaks of methyl groups in hexyl (*b*) and cyclohexyl chains (*b*′), the actual molar ratios of the P3HT and P3cHT segments were calculated to be 63:37 and 77:23 for HcH63 and HcH77, respectively. The composition ratio (*n*:*m*) of HcH is calculated from the ratio of the integrated peak area of *b* to the integrated peak area of *b*′ (Figure S1); [*n*:*m* = (integration of *b*/2):(integration of *b*′)]. We note that the proton resonance at 3.05 and 2.82 ppm are characteristic of α-methylene protons in head-to-tail linkage of 3-alkylthiophene units whereas the proton resonance at 2.59 ppm is characteristic of α-methylene protons in head-to-head or tail-to-tail linkage shown in Figure S1.

HcH63: ^{1}H NMR ($CDCl_3$), δ(ppm): 7.05 (0.37H), 7.0 (0.63H), 3.05–2.59 (1.63H), 1.97–1.70 (2.74H), 1.48–1.36 (6H), 0.96 (2.0H). Regioregularity of HcH63 was calculated to be 91.4%.

HcH77: ^{1}H NMR ($CDCl_3$), δ(ppm): 7.05 (0.23H), 7.0 (0.77H), 3.05–2.58 (1.77H), 1.97–1.70 (2.46H), 1.48–1.36 (6H), 0.96 (2.3H). Regioregularity of HcH77 was calculated to be 94.5%.

Poly(3-cyclohexylthiophene) (P3cHT)

Butylmagnesium chloride (2 M solution in THF, 4.8 mL, 9.6 mmol) was added into a solution of 2,5-dibromo-3-cyclohexylthiophene (3.16 g, 9.8 mmol) in anhydrous THF (40 mL) at 10–15 °C, and purged with N_2. The solution was degassed and purged upon stirring for 30 min at 10–15 °C, then heated at mild reflux for 1 h. Reflux is stopped before the addition of Ni(dppe)Cl_2 (36.2 mg, 0.068 mmol) and then the mixture was refluxed for at least 24 h. The mixture was cooled to room temperature and poured into methanol to form a precipitate. The precipitate was filtered and washed with methanol and hexane, and further purified by Soxhlet extraction in hexane for 2 days. The product was dried in vacuum to yield a black solid. (Yield: 1.04 g, 64.6%). ^{1}H NMR ($CDCl_3$), δ (ppm): 7.05 (1H), 3.05 (0.82H), 2.62 (0.18), 1.97–1.80 (4H), 1.28 (4H), 0.9 (2H). Regioregularity was estimated to be 86%. The polymer has very poor solubility in THF, chloroform, chlorobenzene, 1,2-dichlorobenzene, and etc. The number-average molecular weight (M_n) was determined to be 38,800 g/mol with a polydispersity index of 2.99 by GPC analysis against polystyrene standards in chlorobenzene at 60 °C.

Sample Preparation for TEM and AFM Imaging

HcH63 or HcH77 (15 mg) was dissolved in 1 mL of degassed 1,2-dichlorobenzene (ODCB, Aldrich, anhydrous, 99%) and magnetically stirred overnight at room temperature. The resulting solution was passed through a 1.0 μm filter and allowed to stand for 24 h. For TEM imaging, the solution was diluted 10 times with ODCB, drop-cast onto a TEM grid

(300 mesh, carbon coated, copper grid, Electron Microscopy Sciences) and dried in a vacuum oven. For tapping mode-AFM imaging, the dispersion was spin-coated onto a clean silicon wafer at 3000 rpm and dried in a vacuum oven.

Sample Preparation for WAXS and SAXS

Thick films of HcH63 and HcH77 were first casted from chloroform solutions. The films were annealed at 280 °C under high vacuum for 12 h, and then slowly cooled to room temperature, allowing recrystallization from the melt state.

Characterization

^{1}H NMR spectra were recorded on a Bruker-AF300 spectrometer at 300 MHz. UV–visible absorption spectra were recorded on a Perkin–Elmer model Lambda 900 UV/vis/near-IR spectrophotometer. Spin-coated polymer thin films were prepared from 2 wt % solutions in chloroform. The photoluminescence (PL) emission spectra were obtained with a Photon Technology International (PTI) model QM-2001-4 spectrofluorimeter. The molecular weights reported for the polymers were determined on Polymer Lab Gel Permeation Chromatography (GPC) Model 120 (DRI, PL-BV400HT Viscometer) against polystyrene standards in chlorobenzene at 60 °C. Differential scanning calorimetry (DSC) scans were obtained on TA Instrument Q20 at a heating rate of 10 °C/min.

Small-Angle and Wide-Angle X-Ray Scattering

Small angle X-ray scattering (SAXS) and wide angle X-ray scattering (WAXS) measurements were performed on an Anton-Paar SAXSess instrument. The fixed sample-to-detector distance (265 mm) and wavelength ($\lambda = 0.1542$ nm) provide a comparably limited q-range of 0.2–10 nm^{-1}. Here q is the scattering vector defined as $q = 4\pi\sin(\theta)/\lambda$, with 2θ the scattering angle. The scattering signal was collected by highly sensitive imaging plates and treated by the SAXSquant software from Anton-Paar.

Atomic Force Microscopy

Atomic force microscopy (AFM) imaging was done with a Dimension 3100 Scanning Probe Microscope (Veeco Instruments, Woodbury, NY) operating in tapping mode. The films for atomic force microscopy imaging of surface morphology were spin-coated on a silicon wafer substrate.

Transmission Electron Microscopy

TEM images were acquired on an FEI Tecnai G^2 F20 TEM at 200 kV, with objective aperture to enhance the contrast. TEM images were acquired with a CCD camera and recorded with Gatan DigitalMicrograph^{TM} software.

Fabrication and Characterization of Field-Effect Transistor

Bottom-contact and bottom-gate geometry was used to fabricate and test the field-effect transistors from the copolymers. Heavily n-doped silicon substrates acted as gate electrode and thermally grown silicon dioxide (300 nm thick; $C_i = 11$ nF/cm^2) as gate insulator. Gold source and drain electrodes (50-nm thick) were patterned by photolithography with Cr adhesive layer (~2 nm). Transistor channel has width (W) of 800 μm and length (L) of 20 μm. Substrates were cleaned by ultrasonication with acetone and isopropyl alcohol, and purged with argon. Self-assembled monolayer of octyltrichlorosilane was deposited by vapor deposition. Thin-film was formed from copolymer solution (4 mg/mL in dichlorobenzene) by spin-coating on substrates at 1000 rpm for 120 s, then dried under vacuum at room temperature overnight. Devices were annealed at 150 °C for 1 h under Ar atmosphere. The film thickness was 22–25 nm.

Output (I_{ds} vs. V_{ds}) and transfer (I_{ds} vs. V_g) characteristics of the devices were measured on a Keithley 4200 semiconductor characterization system (Keithley Instruments, Cleveland, OH). Fabrication and characterization of the transistors were done in air except drying and thermal treatment. Field-effect mobility was calculated from the standard equation for saturation region in metal-oxide-semiconductor field-effect transistors: $I_{ds} = \mu(W/2L)C_i(V_g - V_t)$,[2] where I_{ds} is drain-source current, μ is field-effect mobility, W and L are the channel width and length, C_i is the capacitance per unit area of the gate insulator ($C_i = 11$ nF/cm^2), V_g is the gate voltage, and V_t is the threshold voltage.

Fabrication and Characterization of Photovoltaic Cells

Patterned indium tin oxide (ITO) glass substrates (10 Ω per square, Shanghai B. Tree Tech. Consult, Shanghai, China) were cleaned stepwise by acetone, DI water and isopropyl alcohol in an ultrasonic bath. To fabricate the photovoltaic devices, a 50 nm PEDOT buffer layer was spin-coated on top of ITO substrate at 3000 rpm for 30 s and dried at 150 °C for 10 min under vacuum. The blend solutions for active layers were prepared by mixing the polymer (HcH63 or HcH77) with [6,6]–phenyl-C$_{71}$ butyric acid methyl ester (PC$_{71}$BM) and stirred in anhydrous ODCB (30 mg/mL, 1:1 wt:wt), followed by filtration through a 0.45 μm membrane. To prepare blends with different compositions, polymer-to-PC$_{71}$BM weight ratios were kept at 1:0.5, 1:0.75, 1:1, and 1:1.25, respectively. The blends were spin-coated in a N_2 glovebox for 30 s to make thin films with 85–120 nm thickness measured by an Alpha-Step 500 profilometer (KLA-Tencor, San Jose, CA).

Post-treatments of active layers include "film aging" (kept in a closed Petri dish for a certain period of time) and "thermal annealing" (heat treatment on a hot plate for a certain period of time). The as-spin-coated active layer was treated under four conditions. (Condition 1: open dried in glovebox; Condition 2: film aging in a Petri dish until color changes and vacuum dried at 60 °C; Condition 3: film aging in a Petri dish until color changes and thermally annealed at 110 °C for 5 min. Condition 4: film aging in a Petri dish for 30 min and thermally annealed at 110 °C for 30 min.) For composition dependence, the active layers were all treated at Condition 2. The substrates were then loaded into a thermal evaporator (BOC Edwards, 306) for the deposition of the cathode materials. 1.0 nm LiF and 80 nm Al layers were sequentially deposited through a shadow mask on top of the active layer under high vacuum (8×10^{-7} Torr).

Each substrate contained five solar cell devices with an active area of 3.57 mm^2. Current–voltage characteristics of

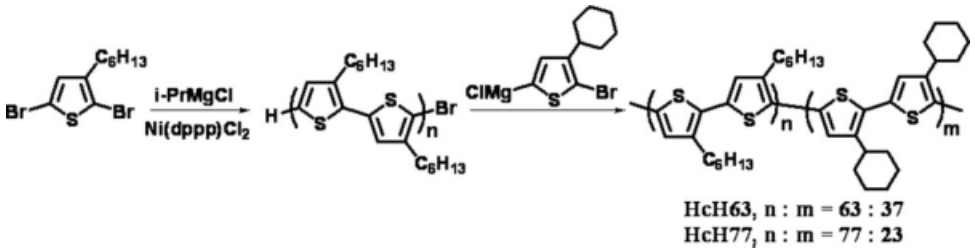

SCHEME 1 Synthesis of Regioregular Poly(3-hexylthiophene)-*b*-poly(3-cyclohexylthiophene).

solar cells were measured using a HP4155A semiconductor parameter analyzer (Yokogawa Hewlett-Packard, Tokyo) in laboratory ambient air condition. A silicon diode (S1787-04, Hamamatsu), calibrated at the National Renewable Energy Lab (NREL, Golden, Colorado), was used to calibrate the filtered Xe lamp. A 100 mW/cm^2 1.5 AM sunlight illumination was simulated for solar cell testing.

The nanoscale morphology in the HcH:$PC_{71}BM$ blend (active layer) thin films was characterized by TEM. To obtain the thin films, the solar cell devices were scratched and soaked in DI water until thin films could be peeled off the substrates. The thin films were then supported on TEM grids (carbon-coated 300 mesh copper grids, Electron Microscopy Sciences) and dried in a vacuum oven overnight. Selected area electron diffraction (SAED) was obtained by using selected area aperture (SAA) with a diameter of 200 μm (0.031 mm^2) and proper exposure time. AFM imaging was performed on the solar cell devices and an area of 5 $\times$ 5 μm^2 on the sample was scanned to study topography and phase on the surface of HcH:$PC_{71}BM$ blend films. UV–visible absorption spectra were recorded on the blend films spin-coated on top of PEDOT/ITO substrates, following the same drying conditions as the corresponding photovoltaic devices.

RESULTS AND DISCUSSION

Synthesis of Poly(3-hexylthiophene)-*b*-poly(3-cyclohexylthiophene)

Synthesis of the diblock copoly(3-alkylthiophene)s and the homopolymer poly(3-cyclohexylthiophene) (P3cHT) was carried out by a modified Grignard metathesis method (GRIM)[41,42,43] as illustrated in Scheme 1. The P3HT block was first synthesized by polymerization of 2,5-dibromo-3-hexylthiophene, followed by the addition of activated 2,5-dibromo-3-cyclohexylthiophene monomer solution, resulting in the diblock copolymer, P3HT-*b*-P3cHT. Two compositions, denoted HcH63 and HcH77, were synthesized by using the molar feed ratios of 2,5-dibromo-3-hexylthiophene to 2,5-dibromo-3-cyclohexylthiophene of 1:1 and 2:1, respectively. The actual compositions of HcH63 and HcH77 were determined from the ^{1}H NMR spectra (Figure S1), based on the α-methylene protons of the hexyl and cyclohexyl side chains which showed resonances at 2.82 and 3.05 ppm, respectively. HcH63 consists of 63 mol % of P3HT block and 37 mol % of P3cHT block. Similarly, HcH77 is composed of 77 mol % of P3HT block and 23 mol % of P3cHT block. So, contrary to the feed ratio the actual compositions revealed a more P3HT block in HcH63 and HcH77. The main reason for this is the poorer solubility of the P3cHT block in the polymerization solvent (THF). Efforts to make other compositions with a greater P3cHT fraction failed. The regioregularity was determined to be 91.4 and 94.5% for HcH63 and HcH77, respectively, based on the resonance of the α-methylene protons.[42]

The weight-average molecular weight (M_w) of HcH63 and HcH77 was 155,500 and 210,800 g/mol, with a polydispersity index (PDI) of 1.45 and 1.57, respectively, determined by gel permeation chromatography (GPC) analysis with polystyrene standards. The GPC traces of the polymers at each step of the block copolymerization are shown in Figure S2 for HcH63. The number-average molecular weights measured by GPC (107,240 g/mol for HcH63 and 134,260 g/mol for HcH77) seem to be much higher than expected M_n from the monomer-to-Ni catalyst ratio (100:1) and this can be explained by over-estimation of measured M_n of poly(3-alkylthiophene)s against polystyrene standards.[44] Although the polydispersity index (1.45–1.57) is quite large compared to conventional block copolymers, it is however similar to that reported for other all-conjugated block copolymers such as poly(3-hexylthiophene)-*b*-poly(3-dodecylthiophene).[43] One possible way to improve the polydispersity is by using asymmetric monomers such as 2-bromo-5-iodo-3-alkylthiophene[38–40] and followed by rigorous purification.[45,46] HcH63 has a lower degree of regioregularity (91.4%) because of the larger P3cHT block fraction. The bulky cyclohexyl side chains appear to hinder the head-to-tail linkage during chain-growth polymerization.[35] Attempts to synthesize P3HT-*b*-P3cHT with a longer block of P3cHT by using HT:cHT ratios of 1:2 and 1:4 were unsuccessful, due to the difficulty in the growth of the P3cHT block that quickly precipitated from solution during polymerization.

Differential scanning calorimetry (DSC) scans of P3cHT homopolymer and P3HT-*b*-P3cHT samples are shown in Figure 1. P3HT has a reported T_m of 240–245 °C,[28] whereas P3cHT (77% regioregularity, $FeCl_3$ oxidation polymerization) was reported to have a T_m of 280–300 °C.[37] A clear melting transition (T_m) and corresponding recrystallization transition (T_c) were observed in P3cHT at 386 °C and 358 °C, respectively. The much higher T_m observed in our sample of P3cHT is a result of both the higher regioregularity and higher molecular weight compared to the literature value.[37] Two distinct T_m values and their corresponding T_c values were seen in the block copolymer samples HcH63 and HcH77. HcH63 showed T_m values of 214 and 363 °C and T_c values of 178 and 276 °C, whereas HcH77 had T_m values of 220 and

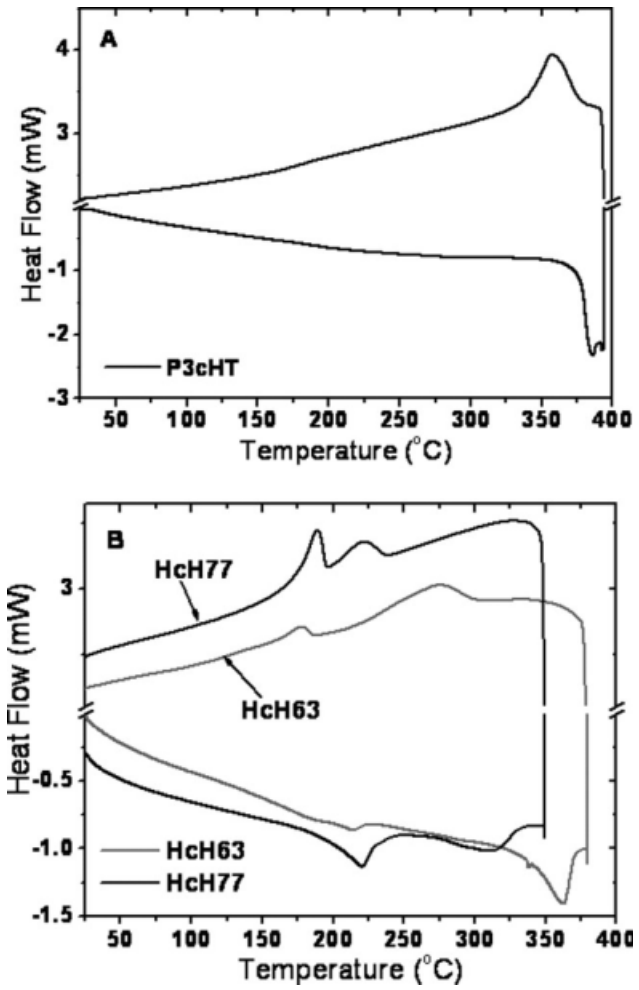

FIGURE 1 (A) The second heating DSC scan of P3cHT. (B) The second heating DSC scans of HcH63 and HcH77.

310 °C and T_c values of 189 and 223 °C. The lower T_m value observed in the DSC scans of each HcH block copolymer sample is due to the P3HT block while the higher T_m value arises from the P3cHT block. The melting transition of the P3HT block in the block copolymers increases from 214 °C in HcH63 to 220 °C in HcH77, which is lower than 240–245 °C observed in the homopolymer P3HT.[28,47] Similarly, the melting transition of the P3cHT block in the block copolymers decreases from 363 °C in HcH63 to 310 °C in HcH77, which is lower than 386 °C seen in the P3cHT homopolymer. The increase of the T_m of each block with increasing amount of that block in the HcH diblock copolymer can be understood in terms of effects of molecular weight and purity on melting transition. These results also confirm the block architecture nature of the HcH samples as observed in other block copolymer systems.[40,48]

Photophysical Properties

The optical absorption spectra of dilute solutions (1.0×10^{-6} M) of HcH63 and HcH77 in chloroform and as spin-coated thin films are shown in Figure 2(A). In chloroform solution, HcH63 and HcH77 had an absorption maximum (λ_{max}) at 469 nm and 453 nm that is similar to the broad and featureless absorption of P3HT.[6] Surprisingly, P3cHT in dilute chloroform solution (1.0×10^{-6} M) showed an absorption maximum at 505 nm and two shoulders at 550 and 610 nm, suggesting the formation of aggregates in solution. Thin films of HcH63 and HcH77 have an identical absorption maximum at 519 nm and shoulder peaks at 550 and 605 nm that are very similar to the P3HT homopolymer.[6] Thin film of P3cHT showed an absorption maximum at 512 nm and two shoulders at 554 and 613 nm, which is more red-shifted compared to that of the film of P3cHT with lower degree regioregularity (λ_{max}: 422 nm).[37] We note that the 605-nm shoulder peak in the absorption spectra of HcH63 and HcH77 films is associated with crystallinity resulting from strong intermolecular interactions (π–π stacking) among regioregular poly(3-alkylthiophene) main chains, in contrast to the blue-shifted absorption seen in regiorandom poly(3-alkylthiophene)s.[28] The optical band gap (E_g^{opt}) of HcH63 and HcH77 estimated from the thin-film absorption edge is 1.91–1.92 eV, which is similar to that of P3HT.[28]

In Figure 2(B), an identical photoluminescence (PL) emission maximum at 578 nm was observed from the PL spectra of

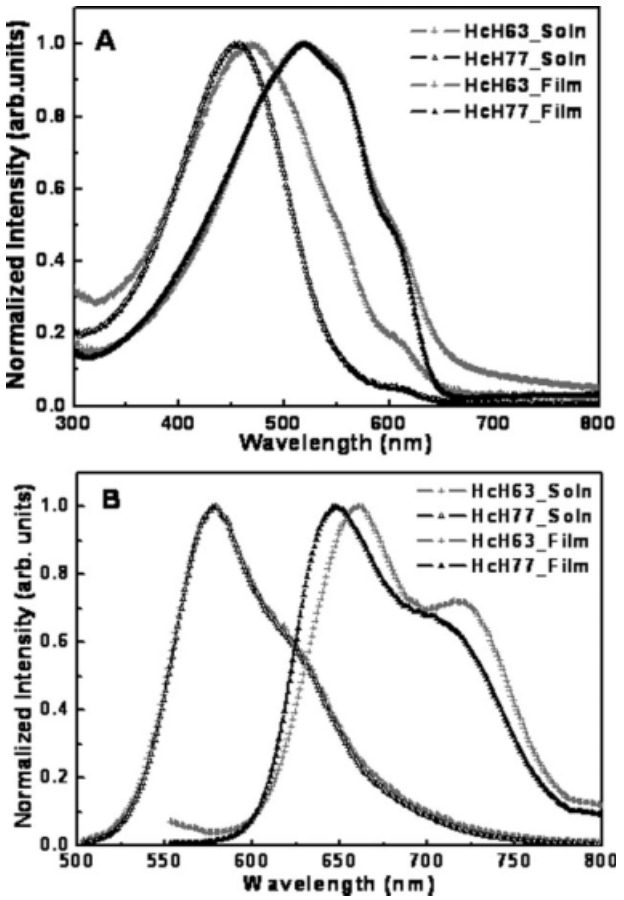

FIGURE 2 Optical absorption (A) and photoluminescence (B) spectra of HcH63 and HcH77 in chloroform solutions and as thin films on glass substrates.

HcH63 and HcH77 solutions in chloroform, which is close to the 570 nm maximum observed in poly(3-alkylthiophene)s, corresponding to the onset of π–π^* transition of the absorption spectra.[28,36] However, no detectable PL emission was obtained from P3cHT solution in chloroform. HcH63 and HcH77 thin films had PL emission maxima at 646–661 nm with shoulder peaks at 710–720 nm which is similar to P3HT. P3cHT thin film had a PL emission maxima at 711 nm, which is much red-shifted compared to the 574-nm emission peak observed in a P3cHT sample with a lower degree of regioregularity.[36] The bulky side chains of P3cHT account for the very similar absorption or photoluminescence spectra in solution and as thin films.[36] On the contrary, P3HT has been known to show a red-shifted absorption and PL emission spectra in the solid state due to the improved electron delocalization in the solid state and good intermolecular ordering in a semicrystalline conjugated polymer.[28] With the attachment of the P3HT block to the P3cHT block, the resulting interchain interaction was improved, which results in the observed red-shifted absorption and PL emission in the thin films of P3HT-*b*-P3cHT.

Microphase Separation and Crystallinity

To investigate the melt-phase behavior and solid-state morphology of HcH63 and HcH77, films spin-casted from chloroform solutions and annealed at 280 °C under high vacuum (10^{-7} mbar, for 12 h) were characterized by wide-angle X-ray scattering (WAXS) and small-angle X-ray scattering (SAXS). Figure 3(A) shows the WAXS spectra of HcH63 and HcH77 and their parent homopolymers, P3HT and P3cHT. Both P3HT and P3cHT exhibit a distinct peak at 3.77 and 4.54 nm^{-1}, respectively. The corresponding d_{100} spacing values observed for P3HT and P3cHT, which are known as the interlayer stacking distance in the crystalline lamellar structure, are 1.67 and 1.38 nm, respectively. The 1.67-nm spacing is known as the interlayer stacking distance in the crystalline lamellar structure of P3HT. The 1.67-nm d_{100} value seen in P3HT based on WAXS is very close to the reported d_{100} of 1.64 nm from X-ray diffraction.[28] For the diblock copolythiophenes HcH63 and HcH77, two scattering vectors in the low-q region (q = 3.72 and 4.48 nm^{-1}) are seen in Figure 3(A), corresponding to the two real-space d_{100} distances of 1.69 nm (d_{P3HT}) and 1.40 nm (d_{P3cHT}), respectively. The relative reflection intensity $I(q^{P3HT})/I(q^{P3cHT})$ correlates with the P3HT/P3cHT block compositions directly. The d_{100} distance (1.69 nm) of the P3HT block is consistent with the model where hexyl side chains are extended and the other smaller d_{100} distance, 1.40 nm, is characteristic of the P3cHT block. The SAXS spectra of HcH63 and HcH77 films, similarly annealed at 280 °C are shown in Figure 3(B). A distinct reflection peak at a scattering vector of 0.38 nm^{-1} is observed in the HcH63 diblock copolymer, corresponding to real space feature of 17.0 nm. Similarly, the low-q reflection peak at 0.31 nm^{-1} observed in the HcH77 corresponds to real space distance of 21.7 nm. The increase in period from HcH63 to HcH77 is consistent with their molecular weights.

The presence of a peak in the low q region for the two block copolymers may arise from two different sources: (i) microphase separation or (ii) density fluctuations observed above an order-disorder transition, also known as correlation hole. The presence of a correlation hole may be ruled out because the extremely low contrast in scattering lengths between P3HT and P3cHT (the two blocks have identical elemental composition, but different architectures) would lead to vanishing small scattering intensities. Furthermore, the crystallinity of the blocks is expected to quench density fluctuations. Finally, the decay slope of the $I(q)$ vs q (not shown here) is consistent with a q^{-3} slope, rather than the q^{-2} behavior expected for a correlation hole.

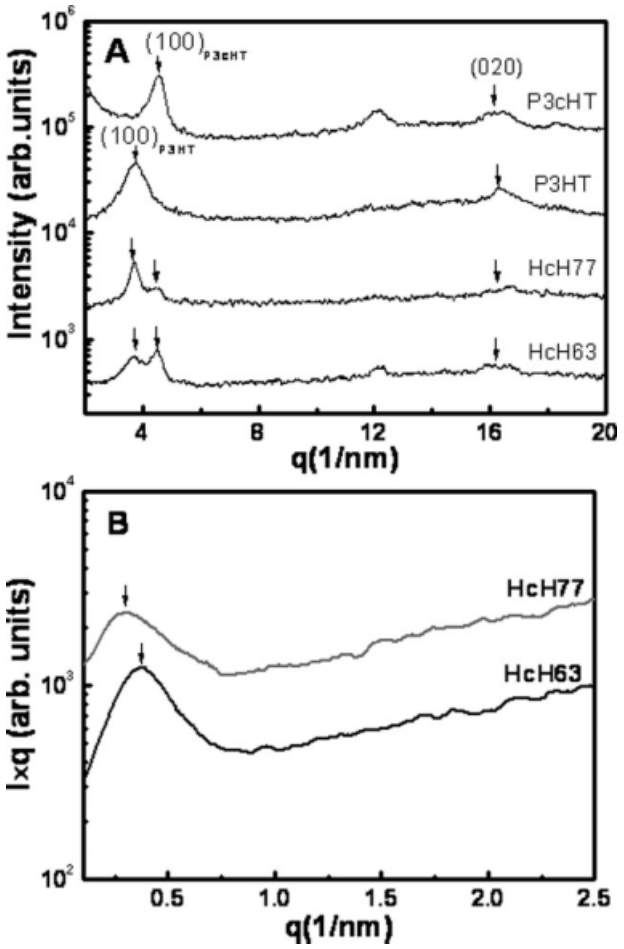

FIGURE 3 (A) WAXS spectra of two homopolymers (P3HT and P3cHT) and two diblock copolymers (HcH63 and HcH77). (B) SAXS spectra of HcH63 and HcH77.

Therefore, combined with the WAXS results from Figure 3(A), these SAXS results strongly support a solid-state assembly of P3HT-*b*-P3cHT into microphase-separated structures with two crystalline domains bearing characteristics of the two different side chains.

Nonetheless, the peak broadness and the q^{-3} decay of the SAXS reflections suggest that the interfaces among microphase-separated domains must be very broad, as compared to perfectly sharp interfaces exhibiting a q^{-4} Porod decay behavior. This is somewhat to be expected for two blocks,

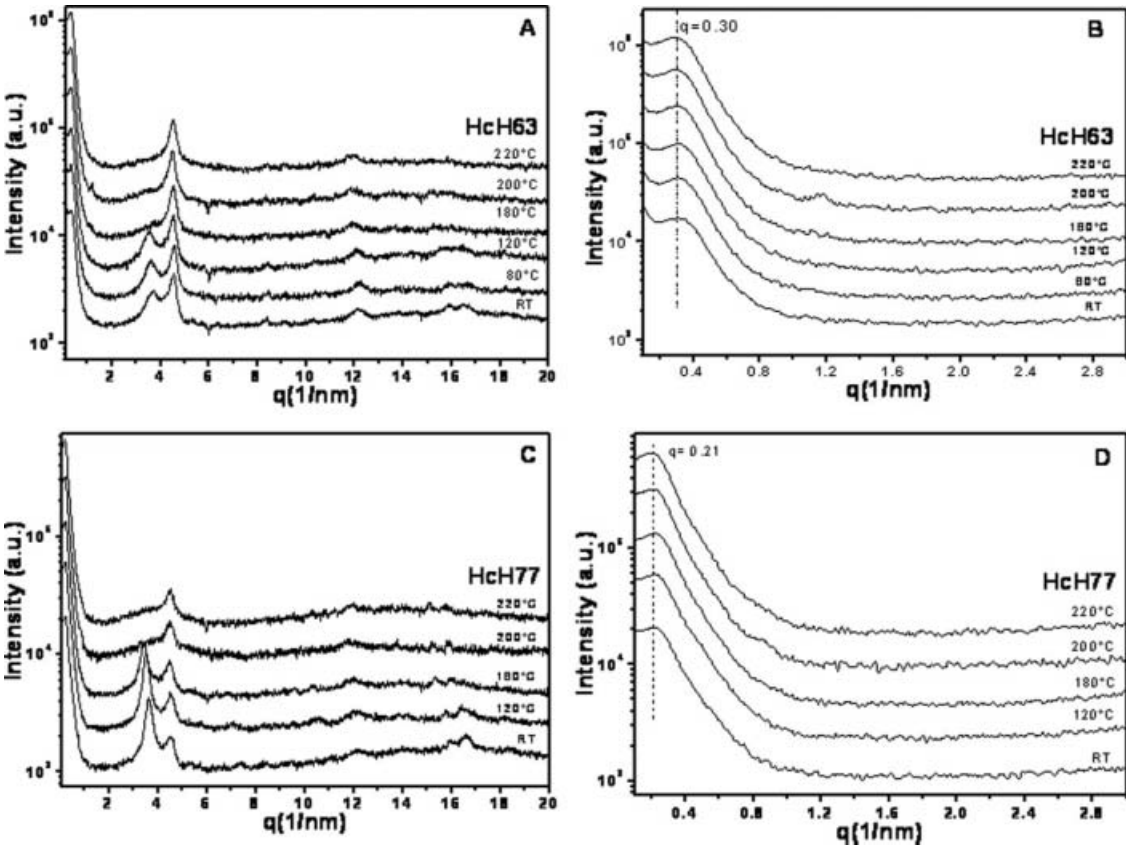

FIGURE 4 Temperature-dependent WAXS and SAXS spectra of HcH63 (A,B) and HcH77 (C,D), respectively.

P3HT and P3cHT, which due to their chemical similarities can only be in a very weakly segregated phase separation regime.

Finally, we note that the period measured by SAXS is consistently smaller than the corresponding contour lengths of the block copolymers estimated from their molecular weights. This implies either a tilted smectic C structure for the microphase separated domains (as expected in similar semicrystalline all-conjugated block copolythiophenes[38]) or a great amount of folding of the chains can also occur. A schematic molecular packing for the P3HT and P3cHT blocks is given in the Supporting Information (Figure S3). The temperature-dependent WAXS and SAXS scans of HcH63 and HcH77 with increasing temperature from room temperature to 220 °C are shown in Figure 4. In the case of HcH63, one of the (100) WAXS reflection corresponding to the P3HT block has gradually decreased with temperature, diminishing into the background signal as the temperature was raised to 180 °C [Fig. 3(A)]. The temperature-dependent presence of the (100) reflection of the P3HT block was observed as the temperature approaches the melting transition of the P3HT block. Similarly, the WAXS scans of HcH77 in Figure 4(C) also show that the (100) reflection of the P3HT blocks is steadily reduced with increasing temperature and finally disappears when the temperature is raised to 200 °C. The transition of the (100) reflection of the P3HT domain, q^{P3HT}, observed in temperature-dependent WAXS scans of HcH63 (~180 °C) and HcH77 (~200 °C) in Figure 4(A,C) is coherent with the onset of their melting transition seen in the DSC scans (Fig. 1), where HcH77 exhibits a higher T_m (219 °C) than HcH63 (206 °C). The corresponding temperature-dependent SAXS scans in Figure 4(B,D) for HcH63 and HcH77, respectively, show that the low-q reflection peaks and thus microphase separation survive up to temperatures beyond the melting transition of P3HT.

Solid-State Morphology

TEM images of drop-cast films from HcH63 and HcH77 solutions from 1,2-dichlorobenzene are shown in Figure 5. HcH63 shows a nanoscale morphology [Fig. 5(A)], whereas HcH77 appears as polymer nanowires with an average width of 12.5 ± 0.9 nm and aspect ratios of 50–120 in Figure 5(B). This is similar to the parent homopolymer P3HT,[49] other poly(3-alkylthiophene)s,[49–51] and poly(3-butylthiophene)-*b*-poly(3-octylthiophene),[41] crystalline polymer chains, which also undergo self-organization into nanowires from solution governed by strong π–π stacking interactions.

The spin-coated diblock copolymer thin films on Si substrate in the fabrication of thin-film transistors were investigated after thermal annealing (150 °C, 1 h) by AFM, as shown in Figure 6. The surface morphology is very similar with average surface roughness of 1.2 nm and 1.3 nm for HcH63 and HcH77, respectively. The domain sizes seen in Figure 6(A,C) are slightly larger than those observed from the thin films

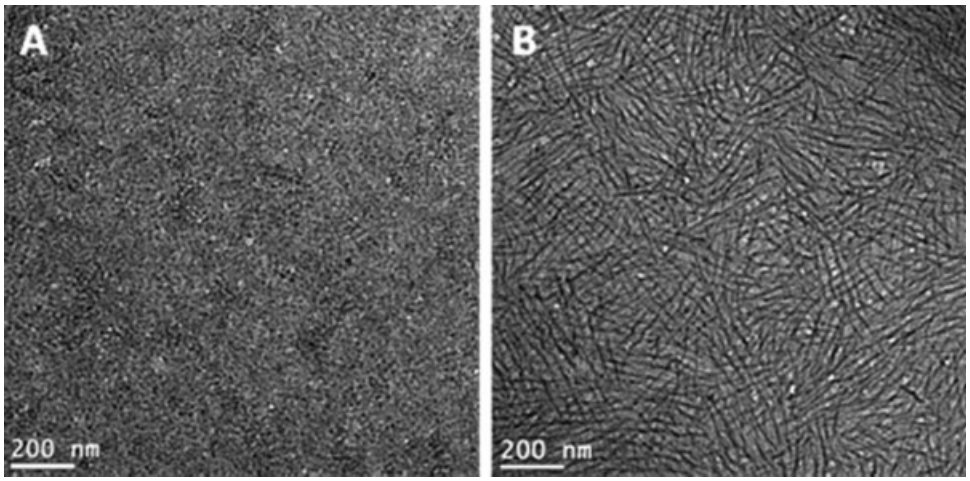

FIGURE 5 TEM images of (A) HcH63 and (B) HcH77 films drop-cast from solutions in 1,2-dichlorobenzene.

before thermal annealing (See Figure S4). Before annealing, the surface roughness is similar (HcH63: 1.4 nm; HcH77: 1.6 nm) in such thin films (22–25 nm). The increase in the domain size may suggest a better molecular connectivity after thermal annealing. Nanowire-like morphology was not observed from the surface of these spin coated copolymer films.

Field-Effect Transistors

Field-effect charge transport in thin films of P3HT-*b*-P3cHT was investigated by fabricating and evaluating bottom-contact and bottom-gate field-effect transistors similar to our previous reports.[23,52,53] Both HcH63 and HcH77 block copolymers showed typical hole-transport characteristics with clear current modulation as shown in Figure 7. HcH77 copolymer showed an average saturation region hole mobility of 1.9×10^{-3} cm^2/Vs which was calculated from transfer curves [Fig. 7(C)].[54] HcH63 showed a lower mobility of 4.5×10^{-4} cm^2/Vs compared to that of HcH77. Current that flows through the channel of HcH77 at on-state is 4- to 5-fold larger compared to that of HcH63. Electrical parameters, such as the mobilities, on/off current ratios, and threshold

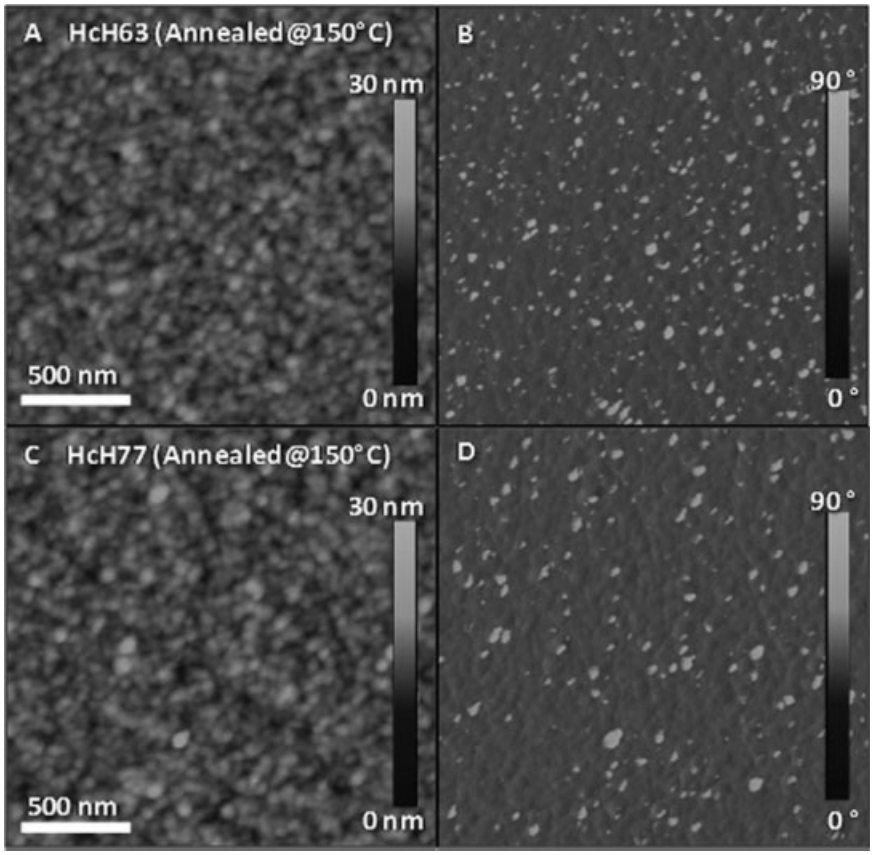

FIGURE 6 Tapping mode AFM topography and phase images of thin films of HcH63 (A,B) and HcH77 (C,D) after thermal annealing at 150 °C for 1 h.

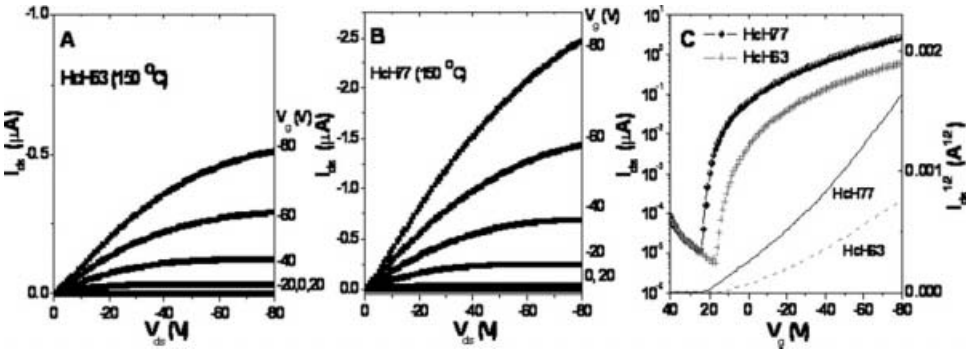

FIGURE 7 Output (A,B) and transfer (C) characteristics of the HcH63 (A) and HcH77 (B) field-effect transistors after thermal treatment at 150 °C for 1 h.

voltages of HcH63 and HcH77 thin films before and after thermal annealing are summarized in Table 1.

The difference in the charge-carrier mobility can be attributed to two different factors. First, the more bulky cyclohexyl side chain can lead to a larger π-stacking distance between polymer backbones. As shown in Figure 3(A), peaks corresponding to [020] plane in P3cHT is slightly shifted to lower q values than in P3HT. Larger distance between π-orbitals prevents efficient charge transport along the π-stacking direction. As HcH63 copolymer has a higher ratio of P3cHT than P3HT blocks, charge transport in HcH63 may be limited by the P3cHT block compared to HcH77. The other possible reason is that the molecular weight of HcH63 is smaller than that of HcH77. It has been reported that the molecular weight significantly affects the hole mobility in P3HT thin films.[47,55,56] Longer polymer chains have more chances of interconnection between highly organized domains, and hence give higher charge-carrier mobility.

The carrier mobility of HcH63 is slightly decreased after thermal annealing at 150 °C, while the mobility of HcH77 remains the same (Table 1). These phenomena can be correlated with temperature dependent WAXS results shown in Figure 4(A,C). HcH63 copolymer showed sudden disappearance of reflection peaks at $q \sim 3.7$ nm^{-1} and $\sim$16 nm^{-1}, characteristics of the crystalline P3HT domain, when the sample was heated from 120 to 180 °C. The reduction of crystallinity can cause the decrease of hole mobility, as crystallinity plays a crucial role for high-mobility in P3HT devices.[57] On the other hand, HcH77 copolymer did not show such sudden transition before 180–200 °C. Therefore, the measured hole mobility is the same before and after thermal annealing at 150 °C.

Off-current of the devices was significantly decreased after thermal annealing, and therefore the on/off current ratio was increased from 10^3 to 10^5 in OFETs based on both HcH63 and HcH77 (Table 1). Threshold voltage also shifted toward negative value upon heat treatment. The increment of on/off ratios and the reduction of threshold voltages after annealing might originate from the removal of dopants (e.g., moisture) which unintentionally doped the films during the device fabrication process in ambient air.

TABLE 1 Field-Effect Charge Transport Properties of Poly(3-hexylthiophene)-*b*-poly(3-cyclohexylthiophene)

Copolymer	Thermal Treatment[a]	Hole Mobility[b] (cm^2/Vs)	$I_{on/off}$[b,c]	V_t[b] (V)
HcH63	–	6.6×10^{-4}	10^3	15
	150 °C for 1 h	4.5×10^{-4}	10^5	−7
HcH77	–	1.9×10^{-3}	10^3	23
	150 °C for 1 h	1.9×10^{-3}	10^5	−2

[a] Thermal treatment was carried out under argon atmosphere.
[b] Average of 12 devices.
[c] Calculated from the ratio of the highest drain current to the lowest drain current in transfer curves.

Photovoltaic Cells

Bulk heterojunction (BHJ) solar cells based on the blends of [6,6]phenyl-C_{71}-butyric acid methyl ester ($PC_{71}BM$) and the diblock copolymers, HcH63 and HcH77, were fabricated and evaluated. All BHJ solar cells had the basic device architecture, ITO/PEDOT:PSS/HcH:$PC_{71}BM$/LiF/Al and were characterized under 100 mW/cm^2 AM1.5 solar irradiation in ambient air. To determine the optimal composition, HcH77:$PC_{71}BM$ blends at four different ratios (1:0.5, 1:0.75, 1:1 and 1:1.25, wt:wt) were investigated in BHJ solar cells. The current density–voltage characteristics of these BHJ devices with different HcH77:$PC_{71}BM$ blend compositions are shown in Figure 8. The corresponding photovoltaic

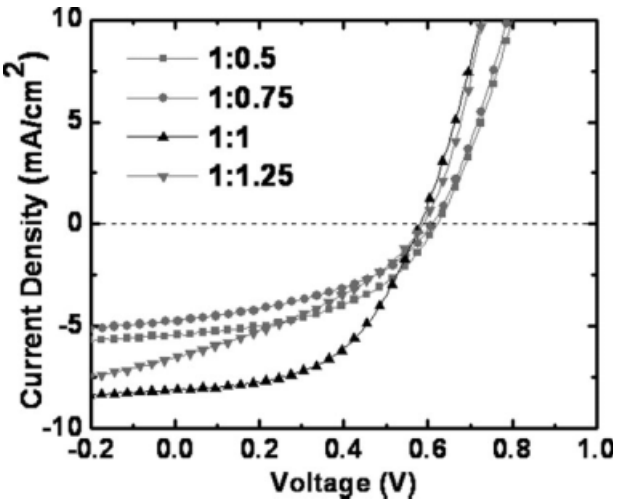

FIGURE 8 Current density–voltage curves of HcH77:$PC_{71}BM$ blend BHJ solar cells at various blend compositions.

TABLE 2 Photovoltaic Parameters of HcH77:$PC_{71}BM$ Blend Solar Cells

Polymer Blend	Composition	Thickness (nm)	V_{oc} (V)	J_{sc} (mA/cm^2)	FF	PCE^{max} (%)	PCE^{avg} (%)
HcH77:$PC_{71}BM$	1:0.5	105	0.62	5.82	0.45	1.63	1.52
	1:0.75	95	0.61	4.69	0.44	1.25	1.11
	1:1	90	0.58	8.14	0.52	2.45	2.37
	1:1.25	100	0.59	6.51	0.36	1.40	1.38

parameters, including open circuit voltage (V_{oc}), short-circuit current density (J_{sc}), fill factor (FF), and power conversion efficiency (PCE) are shown in Table 2.

The thickness of four HcH77:$PC_{71}BM$ blend films was controlled in the range of 90–105 nm after being dried in vacuum. The 0.58–0.62 V open circuit voltages (V_{oc}) observed in the series of HcH77-based BHJ solar cells are very similar to the 0.5–0.6 V typically seen in solar cells based on P3HT.[31,32] The short-circuit current density and fill factor were not ideal, which may arise from the limitations of charge transport in the blend films. The best average PCE (2.37%) was achieved using the HcH77:$PC_{71}BM$ (1:1) blend, with J_{sc} of 8.14 mA/cm^2, V_{oc} of 0.58 V, and quite high FF of 0.52. This result in Table 2 suggests that a 1:1 (wt:wt) ratio of HcH:$PC_{71}BM$ blends is the best composition for the BHJ solar cells, which is in line with the 1:1 best ratio found in the P3HT:$PC_{71}BM$ blend BHJ solar cells reported in the literature.[31,58,59] Thus, we believe the 1:1 ratio is the optimal ratio for balanced charge transport in HcH:$PC_{71}BM$ blend BHJ solar cells, with the limitation of charge transport arising from the relatively low mobility of holes.[60]

The HcH63:$PC_{71}BM$ and HcH77:$PC_{71}BM$ (1:1) blend solar cells under four different post-treatment conditions were tested in air. The four different conditions are: (1) dried in glovebox, (2) film aging in a Petri dish until color changes and then vacuum dried at 60 °C, (3) film aging in a Petri dish until color changes and thermally annealed at 110 °C for 5 min, and (4) film aging in a Petri dish for 30 min and thermally annealed at 110 °C for 30 min. The photovoltaic parameters of BHJ solar cells based on HcH63:$PC_{71}BM$ and HcH77:$PC_{71}BM$ (1:1) blends under these four different post-treatment conditions are summarized in Table 3.

HcH63:$PC_{71}BM$ blend devices achieved a maximum PCE of 1.20% under Condition 2, processed with film aging and vacuum drying. Similarly, HcH77:$PC_{71}BM$ blend devices gave a maximum PCE of 2.45% under Condition 2 (Table 3). The difference in photovoltaic performances between HcH63 and HcH77 devices may be attributed to the molecular weight and the percentage of the P3cHT block in the diblock copolymer. As mentioned earlier, the cyclohexyl rings are more "bulky" compared with linear hexyl chains, and as a result, the close packing of polythiophene backbones along the (020) direction (π–π stacking direction) is affected and is slightly larger than that of P3HT. This explains the observed phenomena that as the percentage of P3cHT block decreases, the charge-carrier mobility increases. Meanwhile, the steric hindrance caused by the "bulky" cyclohexyl side-groups is likely to prevent the close contact between polymer backbones and $PC_{71}BM$ molecules, resulting in reduction of exciton dissociation. As the V_{oc} values (0.58–0.64 V) are very similar in both BHJ devices based on HcH63 and HcH77 in Table 3, the overall low PCEs seen in HcH63:$PC_{71}BM$ blend solar cells are greatly affected by the reduction of J_{sc} and FF and a lower hole mobility of HcH63.

The processing Condition 2 (film aging and then dried in vacuum) seems to be the optimal post-treatment for BHJ devices based on HcH63 and HcH77, without further thermal annealing. Compared with the directly dried devices (Condition 1), the increase of PCE seen in BHJ devices (Condition 2) is largely attributed to the increase of J_{sc}, while FF and V_{oc} is almost identical in both HcH63:$PC_{71}BM$ and HcH77:$PC_{71}BM$ blend devices (Table 3). Such enhancement in polymer solar cell performance during "slow drying" process[31] has been reported, when the molecular order of polymers is improved.[61] The

TABLE 3 Photovoltaic Parameters of HcH63-Based and HcH77-Based Solar Cells

Polymer Blend[a]	Condition[b]	Thickness (nm)	V_{oc} (V)	J_{sc} (mA/cm^2)	FF	PCE^{max} (%)	PCE^{avg} (%)
HcH63:$PC_{71}BM$	1	105	0.64	4.24	0.32	0.86	0.82
	2	**110**	**0.61**	**6.18**	**0.32**	**1.20**	**1.17**
	3	105	0.62	3.85	0.30	0.73	0.71
	4	120	0.63	3.71	0.32	0.74	0.62
HcH77:$PC_{71}BM$	1	90	0.63	6.94	0.51	2.22	2.09
	2	**90**	**0.58**	**8.14**	**0.52**	**2.45**	**2.37**
	3	90	0.63	7.45	0.47	2.18	1.96
	4	85	0.62	7.76	0.50	2.41	2.22

[a] Polymer:$PC_{71}BM$ =1:1 (wt:wt) for all blends.
[b] Condition 1: open dried in glovebox; Condition 2: film aging in a Petri dish until color changes and vacuum dried at 60 °C; Condition 3: film aging in a Petri dish until color changes and thermally annealed at 110 °C for 5 min. Condition 4: film aging in a Petri dish for 30 min and thermally annealed at 110 °C for 30 min.

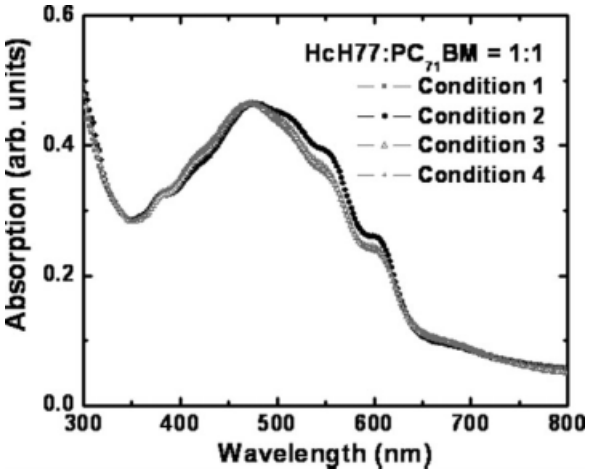

FIGURE 9 UV–visible absorption spectra of HcH77:$PC_{71}BM$ (1:1) blend films at different post-treatment conditions.

improved vibronic shoulders around 560 and 600 nm in HcH77 as observed in the absorption spectra shown in Figure 9, suggest an improved crystallinity in the blend films under Condition 2. Similar enhanced absorption in HcH63:$PC_{71}BM$ blend films is also seen in Figure S5.

In Figure 10, the AFM images of HcH77:$PC_{71}BM$ blend films show that the average surface roughness (R_a) increased from 1.46 nm (Condition 1) to 3.95 nm (Condition 2). Also, the corresponding phase image of the HcH77:$PC_{71}BM$ blend film in Figure 10(D) shows more distinct phase contrast, an indication of increased order and crystallinity in the blend films. In the case of the HcH63:$PC_{71}BM$ blend films, the R_a value changed from 1.68 nm (Condition 1) to 2.04 nm (Condition 2; See Figure S6). During the "slow drying" process (Condition 2), both vertical and horizontal diffusion of $PC_{71}BM$ molecules in polymer films can take place and these two diffusions can be responsible for the increase in surface roughness. The bulky cyclohexyl side chains are more rigid and can affect the diffusion of $PC_{71}BM$ molecules, compared with the flexible linear hexyl side chains. As the solvent evaporates slowly, diffusion of $PC_{71}BM$ molecules takes place and the surface roughness significantly increases, combined with enhanced crystallinity in HcH77:$PC_{71}BM$ films, translating into a higher power conversion efficiency.

TEM imaging was also performed on the HcH:$PC_{71}BM$ blend films peeled directly from the devices, shown in Figure 11 and Figure S7. All films show worm-like nanoscale morphology but the phase contrast between the polymer and $PC_{71}BM$ is better under Condition 2. It should be noted that, in HcH77 devices, the nanowires from solution-phase self-assembly of block copolymers remained intact in the blend films treated under Condition 2, while the nanoscale features are not clear after drying in the glovebox (Condition 1). As the crystalline nanowires contribute to the higher hole mobility, improved exciton dissociation through electrically interconnected pathways, and enhanced performance in photovoltaic devices,[50,51] the nanostructures formed under Condition 2 may be superior than that obtained following Condition 1.

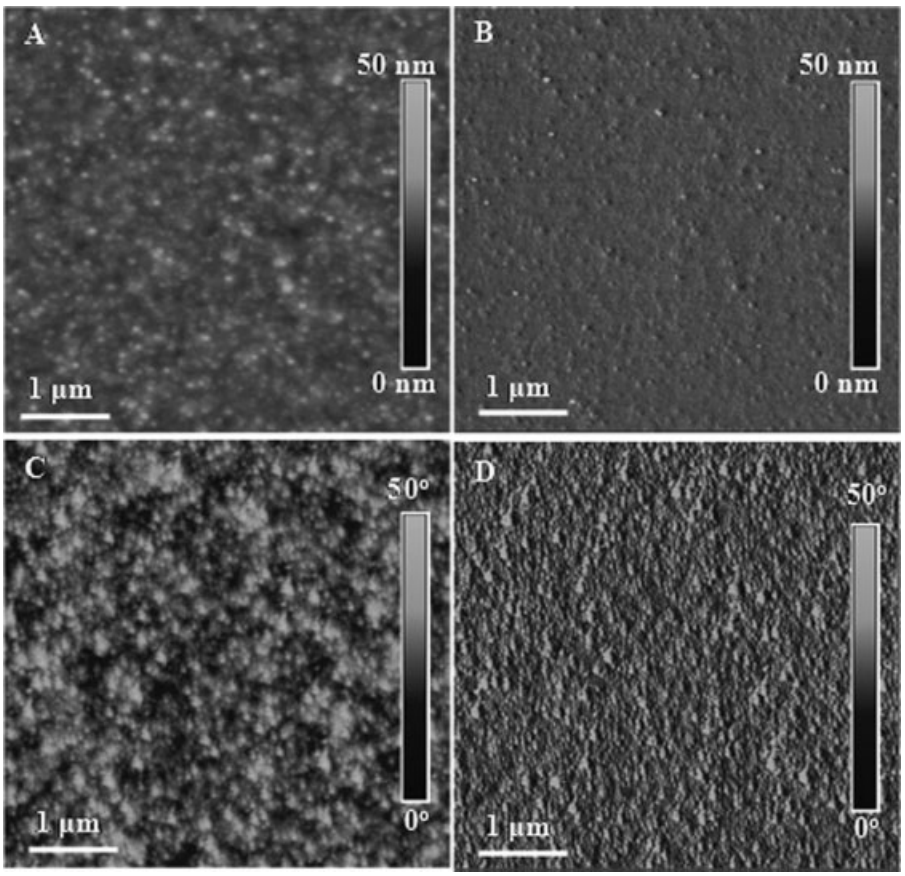

FIGURE 10 AFM images of HcH77:$PC_{71}BM$ (1:1) blend films under Condition 1 (A,B) and Condition 2 (C,D).

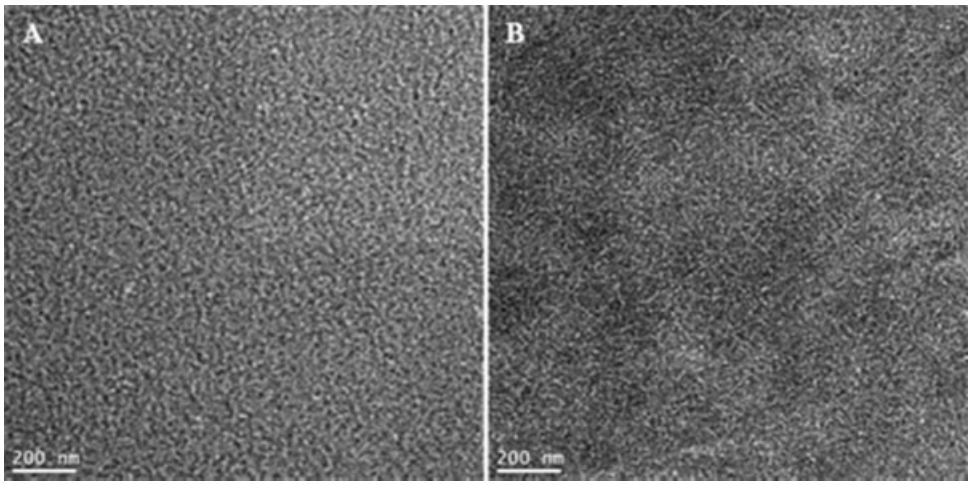

FIGURE 11 TEM images of thin films of HcH77:$PC_{71}BM$ (1:1) blends under different conditions: (A) Condition 1, open dried; (B) Condition 2, film aging and vacuum dried.

Based on selected area electron diffraction (SAED) measurement, it is found that the crystallinity of both polymers and $PC_{71}BM$ is improved with film aging (See Figure S8). These phenomena agree well with the previously discussed results of UV–visible absorption in Figure 9 and AFM and TEM morphology, and might account for the enhancement of photovoltaic performance under Condition 2.

Surprisingly, the commonly applied thermal annealing does not help to increase the performance of HcH:$PC_{71}BM$ solar cells. When comparing BHJ devices obtained under Conditions 2 and 3, the thermal annealing process does not improve the photovoltaic performance (Table 3). J_{sc} in both HcH:$PC_{71}BM$ blends is reduced, and 38% and 8% reductions are observed in HcH63 and HcH77 devices, respectively. During thermal annealing, the fast evaporation of residual solvents allows fast vertical diffusion of $PC_{71}BM$; the "bulky" nature of cyclohexyl ring facilitates this diffusion, and the phase separation in P3HT-*b*-P3cHT/$PC_{71}BM$ blends can be stronger than P3HT/$PC_{71}BM$ blends after heat treatments. With longer film aging time (Condition 4), the residual solvent was nearly completely removed, leaving the sample in a solid state with high crystalline content. Thus, the vigorous heating process does not cause severe vertical phase-separation in that case.

CONCLUSIONS

We have synthesized regioregular poly(3-hexylthiophene)-*b*-poly(3-cyclohexylthiophene) (M_w= 155,500–210,800 g/mol, PDI = 1.45–1.57) and investigated their morphology in the solid state, together with the corresponding electronic, and optoelectronic properties. WAXS and SAXS studies confirmed that the two P3HT-*b*-P3cHT samples in the melt phase assemble into a microphase separated structure with two crystalline domains (length scale ~17.0–21.7 nm) reflecting the two different side chains. Two distinct d_{100} values of 1.40 and 1.69 nm are reflecting the interlayer stacking distance in the crystalline P3cHT and P3HT domains, respectively.

The use of P3HT-*b*-P3cHT as a p-type semiconductor in organic electronics was evaluated by fabricating bottom-contact field-effect transistors and the hole mobility was found to be 4.5×10^{-4} and 1.9×10^{-3} cm^2/Vs for HcH63 and HcH77, respectively. Unlike the parent homopolymer, P3HT, the mobility remains the same after thermal annealing due to the introduction of the more robust P3cHT block. Bulk heterojunction solar cells based on HcH77:$PC_{71}BM$ (1:1) blend films were found to have a 2.45% power conversion efficiency under 100 mW/cm^2 AM1.5 sunlight illumination in ambient air. The slow-drying process (Condition 2) allows the rigid polythiophene chains to self-organize into crystalline structure in the thin films whereas the additional thermal annealing does not further enhance the photovoltaic performance. Our results suggest that block copoly(3-alkylthiophene)s are promising p-type semiconductors, which can be processed without need of additional thermal annealing during device fabrication for organic electronics.

This work was supported by the Department of Energy, Basic Energy Sciences (DE-FG02-07ER46467) and the NSF (DMR-0805259 and DMR-0120967). Part of this work was conducted at the University of Washington NanoTech User Facility, a member of the NSF National Nanotechnology Infrastructure Network (NNIN). C.L. and R.M. thank the Swiss National Science Foundation for financial support.

REFERENCES AND NOTES

1 Babel, A.; Jenekhe, S. A. J Phys Chem B 2003, 107, 1749–1754.

2 Babel, A.; Jenekhe, S. A. Macromolecules 2004, 37, 9835–9840.

3 Alam, M. M.; Tonzola, C. J.; Jenekhe, S. A. Macromolecules 2003, 36, 6577–6587.

4 Zen, A.; Saphiannikova, M.; Neher, D.; Asawapirom, U.; Scherf, U. Chem Mater 2005, 17, 781–786.

5 Sary, N.; Mezzenga, R.; Brochon, C.; Hadziioannou, G.; Ruokolainen, J. Macromolecules 2007, 40, 3277–3286.

6 Jenekhe, S. A.; Chen, X. L. Science 1998, 279, 1903–1907.

7 Alam, M. M.; Jenekhe, S. A. Macromol Rapid Commun 2006, 27, 2053–2059.

8 Zhang, X.; Kale, D. M.; Jenekhe, S. A. Macromolecules 2002, 35, 382–393.

9 Chen, X. L.; Jenekhe, S. A. Science 1999, 283, 372–375.

10 Chen, X. L.; Jenekhe, S. A. Macromolecules 2000, 33, 4610–4612.

11 Liu, J.; Sheina, E.; Kowalewski, T.; McCullough, R. D. Angew Chem Int Ed 2002, 41, 329–332.

12 Leclére, Ph.; Calderone, A.; Marsitzky, D.; Francke, V.; Geerts, Y.; Müllen, K.; Brédas, J.-L.; Lazzaroni, R. Adv Mater 2000, 12, 1042–1046.

13 Stalmach, U.; de Boer, B.; Videlot, C.; Van Hutten, P. F.; Hadziioannou, G. J Am Chem Soc 2000, 122, 5464–5472.

14 Olsen, B. D.; Segalman, R. A. Macromolecules 2005, 38, 10127–10137.

15 Sary, N.; Brochon, C.; Hadziioannou, G.; Mezzenga, R. Eur Phys J E 2007, 24, 379–384.

16 Chen, X. L.; Jenekhe, S. A. Macromolecules 1996, 29, 6189–6192.

17 Scherf, U.; Gutacker, A.; Koenen, N. Acc Chem Res 2008, 41, 1086–1097.

18 Liang, Y.; Wang, H.; Yuan, S.; Lee, Y.; Gan, L.; Yu, L. J Mater Chem 2007, 17, 2183–2194.

19 Plank, H.; Güntner, R.; Scherf, U.; List, E. J. W. Adv Funct Mater 2007, 17, 1093–1105.

20 Tu, G.; Li, H.; Forster, M.; Heiderhoff, R.; Balk, L. J.; Scherf, U. Macromolecules 2006, 39, 4327–4331.

21 Rubatat, L.; Kong, X.; Jenekhe, S. A.; Ruokolainen, J.; Hojeij, M.; Mezzenga, R. Macromolecules 2008, 41, 1846–1852.

22 Sary, N.; Rubatat, L.; Brochon, C.; Hadziioannou, G.; Ruokolainen, J.; Mezzenga, R. Macromolecules 2007, 40, 6990–6997.

23 Zhu, Y.; Champion, R. D.; Jenekhe, S. A. Macromolecules 2006, 39, 8712–8719.

24 Yamamoto, T.; Koizumi, T. Polymer 2007, 48, 5449–5472.

25 Leclére, Ph.; Surin, M.; Brocorens, P.; Cavallini, M.; Biscarini, F.; Lazzaroni, R. Mater Sci Eng R 2006, 55, 1–56.

26 Reddinger, J. L.; Reynolds, J. R. Adv Polym Sci 1999, 145, 57–122.

27 McCullough, R. D.; Lowe, R. D.; Jayaraman, M.; Anderson, D. L. J Org Chem 1993, 115, 904–912.

28 Chen, T.-A.; Wu, X.; Rieke, R. D. J Am Chem Soc 1995, 117, 233–244.

29 Bao, Z.; Dobabalapur, A.; Lovinger, A. J. Appl Phys Lett 1996, 69, 4108–4110.

30 Babel, A.; Jenekhe, S. A. Synth Met 2005, 148, 169–173.

31 Li, G.; Shrotriya, V.; Huang, J. S.; Yao, Y.; Moriarty, T.; Emery, K.; Yang, Y. Nat Mater 2005, 4, 864–868.

32 Ma, W. L.; Yang, C. Y.; Gong, X.; Lee, K.; Heeger, A. J. Adv Funct Mater 2005, 15, 1617–1622.

33 Somanathan, N.; Wegner, G. Acta Polym 1999, 50, 145–150.

34 Saxena, V.; Shirodkar, V. S. J Appl Polym Sci 2000, 77, 1051–1055.

35 Saxena, V.; Prakash, R. Polym Bull 2000, 45, 267–274.

36 Theander, M.; Inganäs, O.; Mammo, W.; Olinga, T.; Svensson, M.; Anderson, M. R. J Phys Chem B 1999, 103, 7771–7780.

37 Anderson, M. R.; Berggren, M.; Gustafsson, G.; Hjertberg, T.; Inganäs, O.; Wennerström, O. Synth Met 1995, 71, 2183–2184.

38 Zhang, Y.; Tajima, K.; Hirota, K.; Hashimoto, K. J Am Chem Soc 2008, 130, 7812–7813.

39 Yokozawa, T.; Adachi, I.; Miyakoshi, R.; Yokoyama, A. High Perform Polym 2007, 19, 684–699.

40 Ohshimizu, K.; Ueda, M. Macromolecules 2008, 41, 5289–5294.

41 Wu, P. T.; Ren, G.; Li, C.; Mezzenga, R.; Jenekhe, S. A. Macromolecules 2009, 42, 2317–2320.

42 Heeny, M.; Zhang, W.; Duffy, W.; McCulloch, I.; Koller, G. Merck Co. World Patent Application, WO2007/059838, 2007.

43 Iovu, M. C.; Sheina, E. E.; Gil, R. R.; McCullough, R. D. Macromolecules 2005, 38, 8649–8656.

44 Liu, J.; Loewe, R. S.; McCullough, R. D. Macromolecules 1999, 32, 5777–5785.

45 Lee, Y.; Fukukawa, K.-I.; Bang, J.; Hawker, C. J.; Kim, J. K. J Polym Sci Part A: Polym Chem 2008, 46, 8200–8205.

46 Zhang, S.; Guo, Y.; Fan, J.; Liu, Y.; Chen, H.-Y.; Yang, G.; Zhan, X.; Liu, Y.; Li, Y.; Yang, Y. J Polym Sci Part A: Polym Chem 2009, 47, 5498–5508.

47 Wu, P.-T.; Xin, H.; Kim, F. S.; Ren, G.; Jenekhe, S. A. Macromolecules 2009, 42, 8817–8826.

48 Ouhib, F.; Hiorns, R. C.; De Bettignies, R.; Bailly, S.; Desbrières, J.; Dargon-Lartigau, C. Thin Solid Films 2008, 516, 7199–7204.

49 Samitsu, S.; Shimomura, T.; Heike, S.; Hashizume, T.; Ito, K. Macromolecules 2008, 41, 8000–8010.

50 Xin, H.; Kim, F. S.; Jenekhe, S. A. J Am Chem Soc 2008, 130, 5424–5425.

51 Xin, H.; Ren, G.; Kim, F. S.; Jenekhe, S. A. Chem Mater 2008, 20, 6199–6207.

52 Babel, A.; Jenekhe, S. A. J Am Chem Soc 2003, 125, 13656–13657.

53 Kim, F. S.; Guo, X.; Watson, M. D.; Jenekhe, S. A. Adv Mater 2009; DOI: 10.1002/adma.200901819.

54 Horowitz, G. Adv Mater 1998, 10, 365–377.

55 Kline, R. J.; McGehee, M. D.; Kadnikova, E. N.; Liu, J. S.; Fréchet, J. M. J.; Toney, M. F. Macromolecules 2005, 38, 3312–3319.

56 Zen, A.; Saphiannikova, M.; Neher, D.; Grenzer, J.; Grigorian, S.; Pietsch, U.; Asawapirom, U.; Janietz, S.; Scherf, U.; Lieberwirth, I.; Wegner, G. Macromolecules 2006, 39, 2162–2171.

57 Sirringhaus, H.; Brown, P. J.; Friend, R. H.; Nielsen, M. M.; Bechgaard, K.; Langeveld-Voss, B. M. W.; Spiering, A. J. H.; Janssen, R. A. J.; Meijer, E. W.; Herwig, P.; de Leeuw, D. M. Nature 1999, 401, 685–688.

58 Chirvase, D.; Parisi, J.; Hummelen, J. C.; Dyakonov, V. Nanotechnology 2004, 15, 1317–1323.

59 Shrotriya, V.; Ouyang, J.; Tseng, R. J.; Li, G.; Yang, Y. Chem Phys Lett 2005, 411, 138–143.

60 Brabec, C. J. Sol Energy Mater Sol Cells 2004, 83, 273–292.

61 Li, G.; Yao, Y.; Yang, H.; Shrotriya, V.; Yang, G.; Yang, Y. Adv Funct Mater 2007, 17, 1636–1644.